



Measurement of Ξ_c^+ production in p Pb collisions at $\sqrt{s_{NN}} = 8.16$ TeV at LHCb

LHCb collaboration[†]

Abstract

A study of prompt Ξ_c^+ production in proton-lead collisions is performed with the LHCb experiment at a center-of-mass energy per nucleon pair of 8.16 TeV in 2016 in p Pb and Pb p collisions with an estimated integrated luminosity of approximately 12.5 and 17.4 nb⁻¹, respectively. The Ξ_c^+ production cross section, as well as the Ξ_c^+ to Λ_c^+ production cross-section ratio, are measured as a function of the transverse momentum and rapidity and compared to the latest theory predictions. The forward-backward asymmetry is also measured as a function of the Ξ_c^+ transverse momentum. The results provide strong constraints on theoretical calculation and are a unique input for hadronization studies in different collision systems.

Published in Phys. Rev. C 109, 044901

© 2024 CERN for the benefit of the LHCb collaboration. CC BY 4.0 licence.

[†]Authors are listed at the end of this paper.

1 Introduction

In hadronic collisions, heavy quarks are produced in hard scattering processes with large momentum transfer. Theoretical predictions based on perturbative quantum chromodynamics (pQCD) describe reasonably well the transverse momentum (p_T) differential charm production cross sections in proton-proton (pp) collisions at different energies [1]. The heavy-flavor hadron cross sections are usually computed using the factorization approach as a convolution of three terms [2]: the parton distribution functions of the colliding particles, the hard-scattering cross section, and the fragmentation function (FF) of heavy quarks into a given heavy-flavor hadron. It is assumed that the FFs are universal between collision systems and energies. At the CERN Large Hadron Collider (LHC), the FFs used to describe the measurements of heavy-flavor hadron production in pp collisions at different center-of-mass energies are tuned on e^+e^- collision data within the framework of pQCD over a wide p_T range. However, evidence of nonuniversal FFs was observed by the LHCb collaboration in a study of the Λ_b^0 baryon to B^- and \bar{B}^0 meson production ratio in pp collisions [3]. Multiple measurements of the relative production of different heavy-flavor hadron species have been made, as they are sensitive probes of FFs.

The measurements of heavy-flavored hadron ratios in hadronic collisions, such as the Λ_c^+/D^0 cross-section ratio, in pp collisions at $\sqrt{s} = 5, 7$ and 13 TeV and in proton-lead (pPb) collisions at $\sqrt{s} = 5$ TeV [4–6], show an enhancement with respect to predictions from pQCD calculations with charm fragmentation based on e^+e^- [7, 8] and e^-p [9–11] measurements. Similar observations were made in the measurement of the Ξ_c^0 (Ξ_c^+)/ D^0 cross section ratio in pp collisions at $\sqrt{s} = 7$ and 13 TeV [12, 13]. Multiple models explain the ratio enhancement. For example, color reconnection [14] could be stronger in pp collisions than in e^+e^- collisions, resulting in an enhanced production of baryons relative to mesons. Other models predicts that hadronization via coalescence [15] will take place.

This paper presents a study of the ratio of production of the Ξ_c^+ particle, a charm-strange baryon, to the production of the Λ_c^+ baryon in pPb collisions at the LHCb experiment. This measurement has the potential to shed light on the mechanism of hadronization and its universality as it is the first one to be performed in proton-nucleus collisions, considered the best environment to study the so-called cold nuclear matter (CNM) effects, such as shadowing [16–18], energy loss [19] and nuclear break-up [20]. In nucleus-nucleus collisions, in addition to CNM effects, experimental results indicate the formation of a high-density color-deconfined medium, the quark-gluon plasma (QGP), a state of matter with asymptotically free partons, which is expected to exist at extremely high temperature and density. The presence of QGP can be determined by observing the change in behavior of the particles as they traverse the nuclear medium with respect to their behavior in the absence of QGP [21]. In pPb collisions the energy density is not expected to be sufficient to produce a QGP medium; however, some theoretical models predict the formation of “QGP droplets” [22], which could partially induce in pPb the same behavior, albeit less pronounced, as in PbPb collisions. Moreover, several QGP models predict that strange (s) quark production is enhanced in heavy-ion collisions, as first reported in Ref. [23]; thus, strangeness enhancement and strange antibaryon abundance are considered signatures for QGP formation [24–26], mainly due to the predominance of the gluonic production mechanism $gg \rightarrow s\bar{s}$. Strangeness enhancement is investigated at accelerators by studying the ratio of production rates of hadrons containing a strange quark to those without, as done, by experiments at CERN [27] and BNL Relativistic

Heavy Ion Collider (RHIC) [28, 29]. The ratio of Ξ_c^+ to Λ_c^+ production measured in this paper, by comparing a baryon with strange content to one without, has the potential to test the presence of QGP formation from QGP droplets in p Pb collisions, which has not yet been established.

2 Analysis, detector, and simulation

The Ξ_c^+ and Λ_c^+ candidates¹ in the analysis are reconstructed via the hadronic decay to the $pK^-\pi^+$ final state. The measurements are performed as a function of p_T and rapidity (y^*) of the baryons, using p Pb and Pb p collisions with an estimated integrated luminosity of approximately 12.5 and 17.4 nb⁻¹ [30], respectively, collected by the LHCb detector at center-of-mass energy per nucleon pair of $\sqrt{s_{NN}} = 8.16$ TeV. The rapidity y^* in the nucleon-nucleon center-of-mass system is related to the rapidity in the laboratory frame (y_{lab}) via $y^* = y_{\text{lab}} \pm 0.4645$. Here, 0.4645 is the shift in rapidity in the direction of the proton beam due to the unequal mass of the two colliding objects. The proton beam and the lead beam have different energies per nucleon in the laboratory frame, with $E_p = 6.5$ TeV and $E_{\text{Pb}} = 2.56$ TeV. The particles are separated according to whether they originate from the collision point (prompt) or from the decay of b hadrons (nonprompt) using the impact parameter (IP), defined as the distance of closest approach of the particle trajectory to the collision point. Data are analyzed separately in the p Pb (forward) sample, covering a rapidity range $1.5 < y^* < 4.0$, and the Pb p (backward) sample, covering the range $-5.0 < y^* < -2.5$.

The double differential cross section for prompt Ξ_c^+ (Λ_c^+) production is measured as

$$\frac{d^2\sigma_{\Xi_c^+(\Lambda_c^+)}(p_T, y^*)}{dp_T dy^*} = \frac{N_{\Xi_c^+(\Lambda_c^+)}(p_T, y^*)}{\mathcal{L} \cdot \mathcal{B} \cdot \epsilon_{\text{tot}}(p_T, y^*) \cdot \Delta p_T \Delta y^*}, \quad (1)$$

where $N_{\Xi_c^+(\Lambda_c^+)}(p_T, y^*)$ is the measured signal yield of prompt Ξ_c^+ (Λ_c^+) decays produced in a given interval of p_T and y^* , Δp_T and Δy^* , respectively, and \mathcal{L} represents the integrated luminosity. The branching fractions \mathcal{B} are $(0.62 \pm 0.30)\%$ and $(6.28 \pm 0.32)\%$, for the decays $\Xi_c^+ \rightarrow pK^-\pi^+$ and $\Lambda_c^+ \rightarrow pK^-\pi^+$, respectively [31]. Finally, $\epsilon_{\text{tot}}(p_T, y^*)$ stands for the total signal efficiency determined in the Δp_T and Δy^* interval. The production ratio of Ξ_c^+ to Λ_c^+ , $R_{\Xi_c^+/\Lambda_c^+}(p_T, y^*)$, is defined as

$$R_{\Xi_c^+/\Lambda_c^+}(p_T, y^*) \equiv \frac{d^2\sigma_{\Xi_c^+}(p_T, y^*)/dp_T dy^*}{d^2\sigma_{\Lambda_c^+}(p_T, y^*)/dp_T dy^*}. \quad (2)$$

The forward-backward asymmetry, $R_{\text{FB}}(p_T, y^*)$, is measured in the overlapping rapidity range $2.5 < |y^*| < 4.0$ and is defined as

$$R_{\text{FB}}(p_T, y^*) \equiv \frac{d^2\sigma_{\Xi_c^+}(p_T, +|y^*|)/dp_T dy^*}{d^2\sigma_{\Xi_c^+}(p_T, -|y^*|)/dp_T dy^*}. \quad (3)$$

The LHCb detector [32, 33] is a single-arm forward spectrometer covering the pseudorapidity range $2 < \eta < 5$, designed for the study of particles containing b or

¹Charge conjugate decays are implied throughout this paper, unless otherwise stated.

c quarks. The detector includes a high-precision tracking system consisting of a silicon-strip vertex detector surrounding the pp interaction region [34], a large-area silicon-strip detector located upstream of a dipole magnet with a bending power of about 4 Tm, and three stations of silicon-strip detectors and straw drift tubes [35] placed downstream of the magnet. The tracking system provides a measurement of the momentum, p , of charged particles with a relative uncertainty that varies from 0.5% at low momentum to 1.0% at 200 GeV/ c . The minimum distance of a track to a primary pp collision vertex (PV), the impact parameter (IP), is measured with a resolution of $(15 + 29/p_T)$ μm , where p_T is the component of the momentum transverse to the beam, in GeV/ c . The different types of charged hadrons, such as the kaons and pions used in this analysis, are distinguished using information from two ring-imaging Cherenkov detectors [36]. Photons, electrons and hadrons are identified by a calorimeter system consisting of scintillating-pad and preshower detectors, an electromagnetic and a hadronic calorimeter. Muons are identified by a system composed of alternating layers of iron and multiwire proportional chambers [37]. The online event selection is performed by a trigger [38], which consists of a hardware stage, based on information from the calorimeter and muon systems, followed by a software stage, which applies a full event reconstruction.

Simulation is used to model the reconstruction efficiency and the effects of the selection requirements. Charmed baryons are generated in pp collisions at $\sqrt{s} = 8.16$ TeV using the PYTHIA [39] generator and are embedded into the EPOS [40] generator, which simulates the environment of the proton-lead collision. Particle decays are described by EVTGEN [41], while the interaction of particles with the detector, and its response in simulation, are implemented using the GEANT4 toolkit [42, 43].

3 Candidate selection

The online event selection is performed by a trigger, which consists of a hardware stage followed by a two-level software stage. In between the two software stages, an alignment and calibration of the detector is performed in near real-time and their results are used in the trigger [44]. The same alignment and calibration information is propagated to the offline reconstruction, ensuring consistent and high-quality particle identification (PID) information between the trigger and offline software. The identical performance of the online and offline reconstruction offers the opportunity to perform physics analyses directly using candidates reconstructed in the trigger [38, 45] which the present analysis exploits. The Ξ_c^+ and Λ_c^+ baryons are reconstructed by combining three tracks identified as proton, kaon and pion candidates. All the charged tracks are required to be well reconstructed and to have transverse momentum $p_T > 400$ MeV/ c and be incompatible with originating at the PV. The tracks must also be within the LHCb acceptance $2.0 < \eta < 5.0$ and in the kinematic range $3.2 < p < 100.0$ GeV/ c . The Ξ_c^+ and Λ_c^+ candidates are required to have a good quality secondary vertex and a reconstructed decay time between 0.1 and 10 ps. The angle between the reconstructed candidate momentum and the vector pointing from the PV to the secondary vertex is required to be close to zero. The $pK^-\pi^+$ invariant mass is required to be within ± 70 MeV/ c^2 of the known Ξ_c^+ (Λ_c^+) mass [31]. The invariant mass resolution for the reconstructed candidates is around 10 MeV/ c^2 .

4 Determination of signal yields and efficiency

The signal yields are determined using a maximum-likelihood fit to the $pK^-\pi^+$ invariant mass distributions, which were verified to be independent of the other kinematic variables. The signal component of the fit model is represented by a sum of a Crystal Ball function [46] and a Gaussian function, which share a common mean value. The background component is described by a linear function. The results of the invariant mass fits for Ξ_c^+ and Λ_c^+ in $p\text{Pb}$ and $\text{Pb}p$ data samples are shown in Fig. 1.

The obtained signal yields are about 13.3×10^3 (12.6×10^3) Ξ_c^+ decays and 119.2×10^3 (104.4×10^3) Λ_c^+ decays in the $p\text{Pb}$ ($\text{Pb}p$) sample after background subtraction, achieved using the *sPlot* technique [47] with the $pK^-\pi^+$ invariant mass as the discriminating variable. The extracted signal contains promptly produced baryons and nonprompt signal from the decay of b hadrons. To extract the prompt component, the method developed in Ref. [6] is used, with the variable χ_{IP}^2 discriminating between prompt and nonprompt production. The χ_{IP}^2 variable is defined as the difference in the vertex-fit χ^2 of a given PV reconstructed with and without the Ξ_c^+ (Λ_c^+) candidate under consideration. The prompt and nonprompt components are modelled with a Bukin function [48]. The asymmetry parameters of the Bukin function describing the prompt component are fixed using results

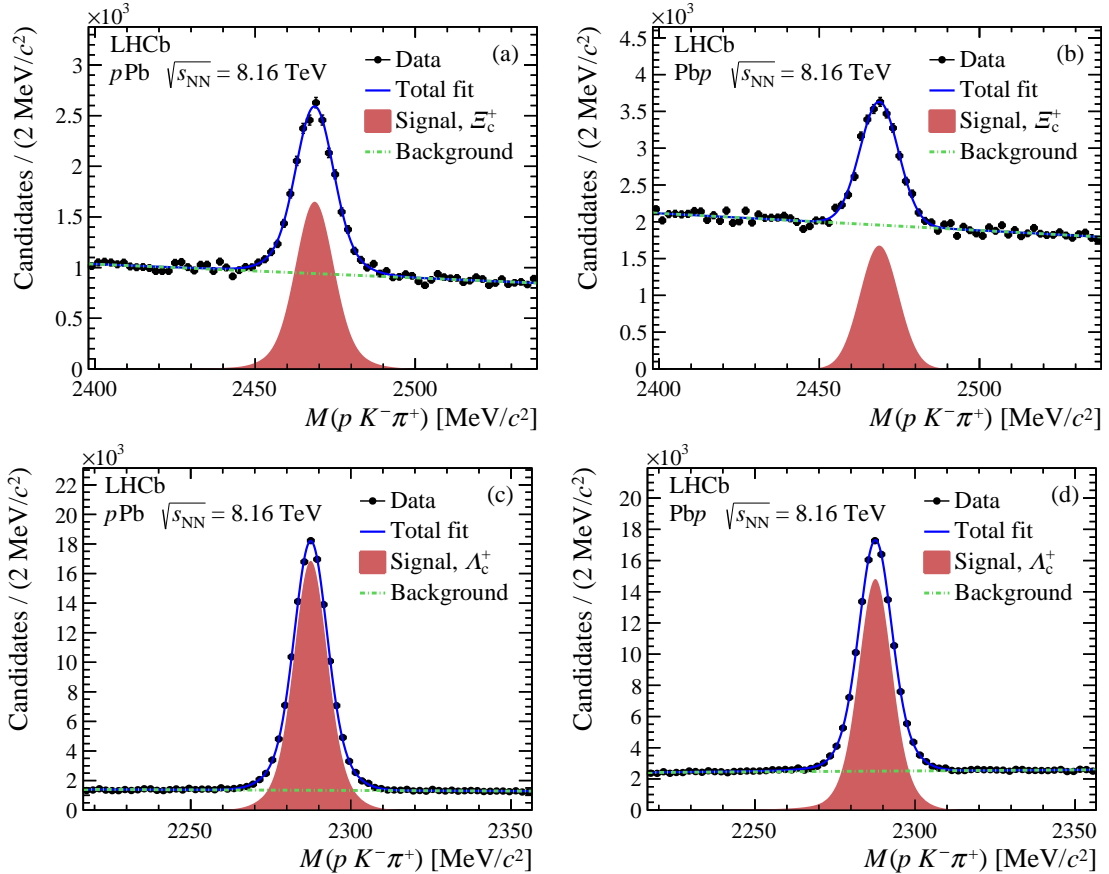


Figure 1: Invariant mass distributions for (a) Ξ_c^+ candidates in $p\text{Pb}$ data, (b) Ξ_c^+ candidates in $\text{Pb}p$ data, (c) Λ_c^+ candidates in $p\text{Pb}$ data, and (d) Λ_c^+ candidates in $\text{Pb}p$ data. The results of the fit are overlaid.

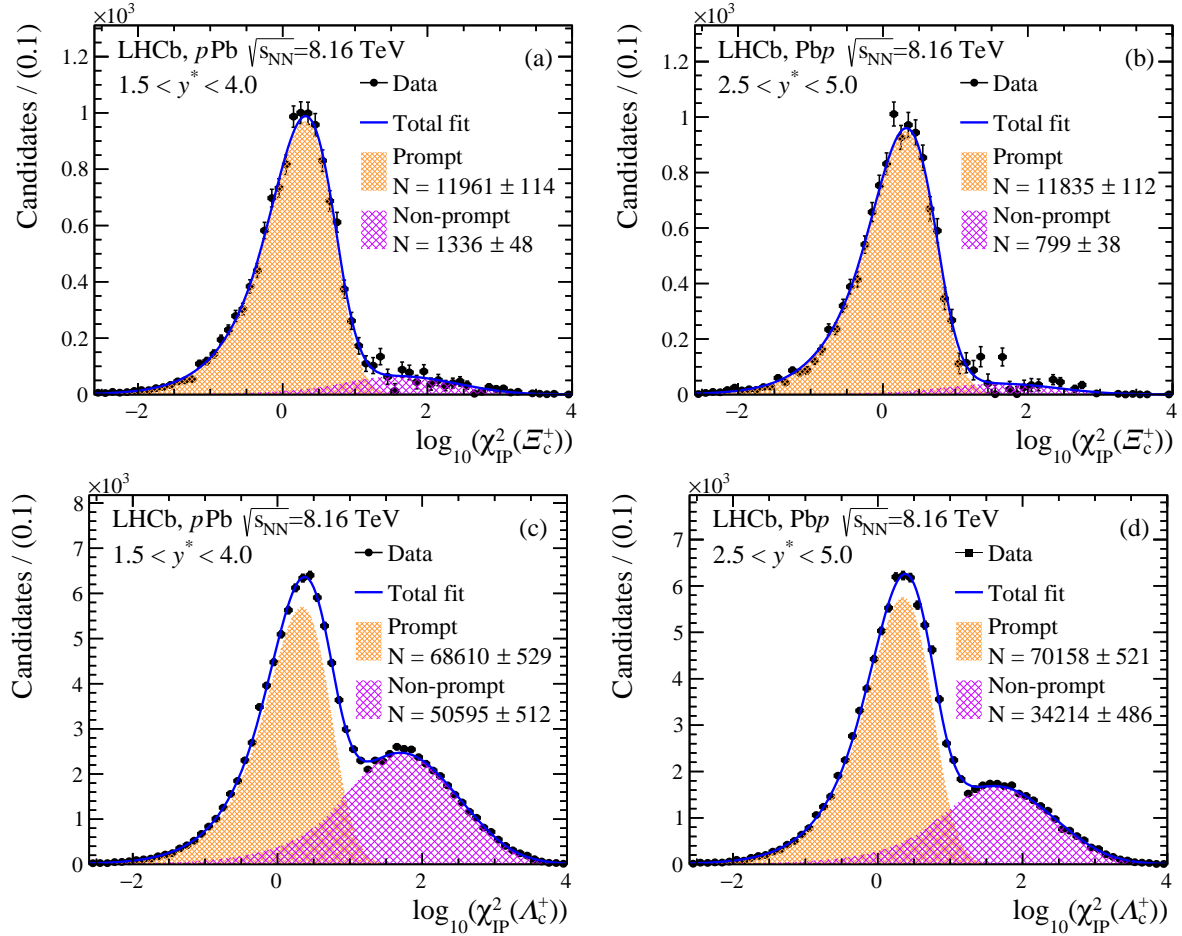


Figure 2: Background-subtracted $\log_{10}(\chi_{\text{IP}}^2)$ distributions of (a) Ξ_c^+ and (b) Λ_c^+ candidates in (left) $p\text{Pb}$ and (right) $\text{Pb}p$ data. The results of the fit are overlaid.

from fits to simulated samples. The results of the background-subtracted distribution fits of the $\log_{10}(\chi_{\text{IP}}^2)$ for Ξ_c^+ and Λ_c^+ in $p\text{Pb}$ and $\text{Pb}p$ data samples are shown in Fig. 2. The quantity $N^{\Xi_c^+ (\Lambda_c^+)}(p_{\text{T}}, y^*)$ is obtained by performing the invariant mass and $\log_{10}(\chi_{\text{IP}}^2)$ fits in each (p_{T}, y^*) bin.

Simulated data are used to determine the total efficiency, defined as the product of the geometrical acceptance of the detector, and the reconstruction, selection, PID and trigger efficiencies. The samples are weighted to match the background-subtracted data using the distributions of p_{T} , y^* , the number of VELO clusters and the invariant mass of the pK^- and $K^-\pi^+$ combinations. The PID efficiency is also measured with dedicated calibration data samples [49].

5 Systematic uncertainties

Several sources of systematic uncertainty are studied. A systematic uncertainty in the signal yield determination is evaluated by changing the function used in the fit for the nonprompt component, switching from a Bukin function to a Gaussian. The difference in the signal yields obtained with the two fits is taken as a systematic uncertainty. The systematic uncertainty associated to the background determination, which is dominant, is

Table 1: Summary of systematic uncertainties on the Ξ_c^+ and Λ_c^+ cross sections in p_T bins in the pPb and PbP samples. The range of uncertainties correspond to the values obtained for different bins of p_T .

	Ξ_c^+		Λ_c^+	
	pPb	PbP	pPb	PbP
Signal	0.1–2.2 %	0.2–2.3 %	–	–
Background	1.3–5.7 %	0.5–18.0 %	0.1–1.0 %	0.1–0.8 %
ε_{acc}	0.1–0.2 %	0.1–0.3 %	0.1–0.2 %	0.1–0.2 %
$\varepsilon_{\text{sel/rec}}$	1.1–3.5 %	1.3–4.8 %	3.6–7.3 %	2.7–5.5 %
ε_{PID}	0.3–0.7 %	0.6–1.4 %	0.2–0.6 %	0.5–1.1 %
$\varepsilon_{\text{trg/sel}}$	0.4–0.5 %	0.4–0.5 %	0.1–0.6 %	0.4–0.8 %
Total	2.0–6.3 %	2.9–18.0 %	3.6–7.3 %	2.8–5.6 %

Table 2: Summary of systematic uncertainties on the Ξ_c^+ and Λ_c^+ cross sections in y^* bins in the pPb and PbP samples. The range of uncertainties correspond to the values obtained for different bins of y^* .

	Ξ_c^+		Λ_c^+	
	pPb	PbP	pPb	PbP
Signal	0.2–3.0 %	0.2–3.6 %	2.0–5.9 %	–
Background	0.1–5.7 %	1.7–27.4 %	0.1–4.6 %	0.7–17.7 %
ε_{acc}	0.1–0.4 %	0.1–0.8 %	0.1–0.3 %	0.1–0.5 %
$\varepsilon_{\text{sel/rec}}$	0.7–2.8 %	1.5–4.2 %	3.4–6.8 %	1.2–14.4 %
ε_{PID}	0.4–1.5 %	0.5–3.0 %	0.2–2.3 %	0.4–3.8 %
$\varepsilon_{\text{trg/sel}}$	0.4–0.5 %	0.4–0.6 %	0.4–0.5 %	0.4–1.2 %
Total	1.6–6.4 %	2.7–27.8 %	4.1–9.9 %	1.8–17.9 %

evaluated by using a sideband subtraction technique, instead of the *sPlot* method. The uncertainties in reconstruction, selection, and PID efficiencies are evaluated by varying the reweighting procedure by excluding the distributions of the invariant mass of the pK^- and $K^-\pi^+$ combinations. The uncertainties in the branching fractions are accounted for. Summaries of the systematic uncertainties in the Ξ_c^+ and Λ_c^+ cross sections can be found in Tables 1, 2, and 3.

6 Results

In this section the different measurements performed are discussed. More results can be found in the Appendix.

Table 3: Summary of systematic uncertainties correlated among bins on the Ξ_c^+ and Λ_c^+ cross sections in the $p\text{Pb}$ and $\text{Pb}p$ samples.

	$p\text{Pb}$	$\text{Pb}p$
Luminosity	2.6 %	2.5 %
Signal	4.8 %	2.8–3.1 %
Tracking	5.5%	
$\mathcal{B}(\Xi_c^+ \rightarrow p^+ K^- \pi^+)$	48.4%	
$\mathcal{B}(\Lambda_c^+ \rightarrow p^+ K^- \pi^+)$	5.1%	

6.1 Double-differential cross section

The double-differential cross sections of prompt Ξ_c^+ production times $\mathcal{B}(\Xi_c^+ \rightarrow pK^- \pi^+)$ in proton-lead collisions at $\sqrt{s_{NN}} = 8.16$ TeV are measured as a function of p_T integrated over y^* in the regions $1.5 < y^* < 4.0$ and $-5.0 < y^* < -2.5$, and as a function of y^* integrated over the p_T range between 2.0 and 12.0 GeV/ c . The double-differential cross sections of prompt Ξ_c^+ production are shown in Fig. 3. The data are compared with theoretical predictions [50–52] from the HELAC-Onia method [53, 54] called EPPS16 [55] with three factorization scale choices. The data agree with the predictions and appear to be best described using the scale $0.5\mu_0$. For the forward and backward regions, the integrated cross sections are

$$\begin{aligned} \sigma_{\Xi_c^+}^{p\text{Pb}}(2 < p_T < 12 \text{ GeV}/c, 1.5 < y^* < 4.0) &= 9.69 \pm 0.12 \pm 0.26 \pm 4.72 \text{ mb}, \\ \sigma_{\Xi_c^+}^{\text{Pb}p}(2 < p_T < 12 \text{ GeV}/c, -5.0 < y^* < -2.5) &= 8.10 \pm 0.11 \pm 0.72 \pm 3.95 \text{ mb}, \end{aligned}$$

where the first uncertainty is statistical, the second is the uncorrelated systematic uncertainty and the third is the systematic uncertainty fully correlated among bins.

6.2 Forward-backward asymmetry

The forward-backward ratio R_{FB} , defined in Eq. (3) and measured as a function of p_T , is shown in Fig. 4. The ratio is independent of p_T and agrees with the theoretical prediction within one standard deviation.

6.3 Differential ratio of Ξ_c^+ to Λ_c^+ (D^0)

The differential ratio of Ξ_c^+ to Λ_c^+ production is measured as a function of the number of clusters reconstructed in the VELO ($N_{\text{clusters}}^{\text{VELO}}$) and given in Fig. 5. The ratios are constant as a function of $N_{\text{clusters}}^{\text{VELO}}$, similarly for the $p\text{Pb}$ and $\text{Pb}p$ data, and the results show no indication of strangeness enhancement.

Since LHCb has already measured the D^0 production cross section in $p\text{Pb}$ collisions at $\sqrt{s} = 8.16$ TeV [56], it is also possible to compute the Ξ_c^+/D^0 production ratio. The differential ratios of Ξ_c^+ to Λ_c^+ production and Ξ_c^+ to D^0 production are shown in Fig. 6 as a function of p_T . Both the Ξ_c^+/Λ_c^+ and Ξ_c^+/D^0 ratios show no significant p_T dependence, similarly for the $p\text{Pb}$ and $\text{Pb}p$ data samples. This result provides a strong indication

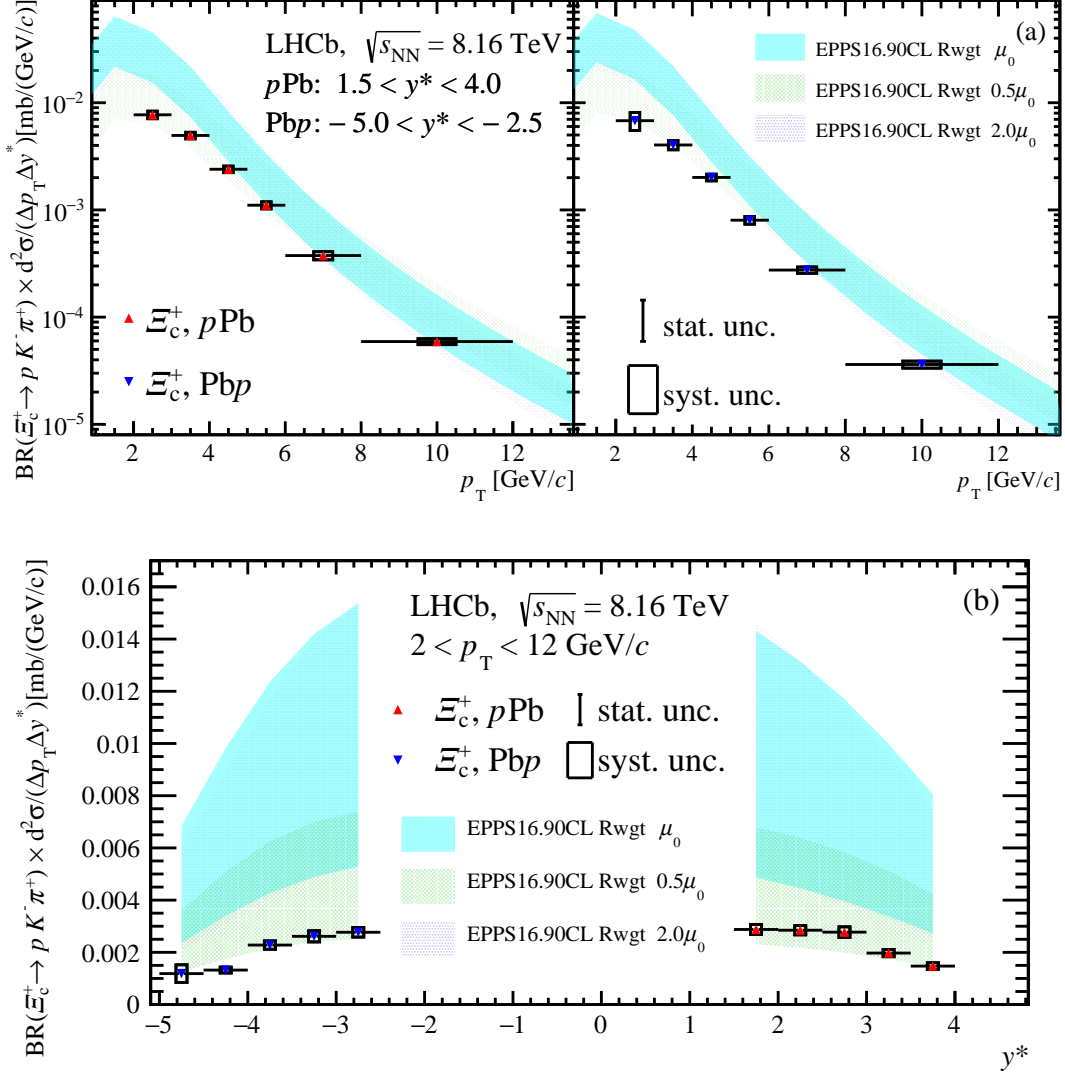


Figure 3: Double-differential cross section of the prompt Ξ_c^+ baryon times $\mathcal{B}(\Xi_c^+ \rightarrow pK^-\pi^+)$ in proton-lead collisions as a function of (a) p_T and (b) y^* in $p\text{Pb}$ (red triangles) and Pbp (blue triangles) collisions. The error bars represent the statistical uncertainties, while the black squares represent the total systematic uncertainties which include correlations among bins.

that the same processes govern hadronization in $p\text{Pb}$ and Pbp collisions. This is the first time they are measured in this system. The data are compared with EPPS16 nPDF predictions [55], which uses the cross section measured in pp collisions by ALICE [13] as input for their calculation. The EPPS16 model shows a similar trend as the data, but significantly overestimates it. The measurements are also compared with results from the PYTHIA 8.3 event generator with a tune that implements color reconnection (CR) beyond the leading-color approximation [14] and the computation obtained with EPOS4HQ, the heavy quark extension of the new EPOS4 framework [4]. Both computations are based on results in pp collisions. The Ξ_c^+/Λ_c^+ cross section ratio is best described by the EPOS4HQ model within uncertainties, despite showing a different trend, especially at low p_T . This behavior is even more pronounced in the Ξ_c^+/D^0 cross section ratio. The Ξ_c^+ to D^0

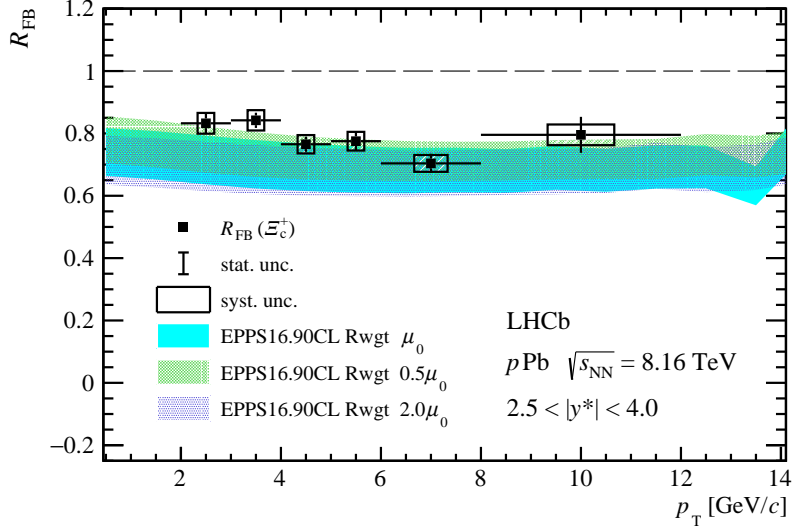


Figure 4: Forward-backward ratio of Ξ_c^+ production as a function of p_T . The error bars represent the statistical uncertainties, while the boxes indicate the systematic uncertainty.

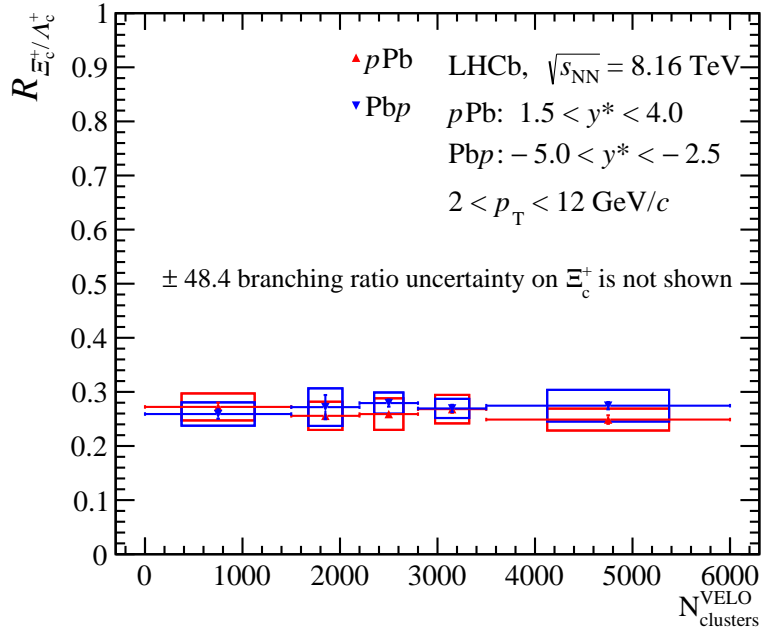


Figure 5: Ratio of prompt Ξ_c^+ to Λ_c^+ production in pPb (red triangles) and PbP (blue triangles) data samples as a function of $N_{clusters}^{VELO}$. The error bars represent the statistical uncertainties, while the squares indicate the systematic uncertainty. The branching ratio uncertainty on Ξ_c^+ is not shown.

production ratio is also compared with the result of ALICE at $\sqrt{s} = 13$ TeV at $|y| < 0.5$ in pp collisions [13]. The ALICE result is generally higher, but the two measurements agree within the uncertainties.

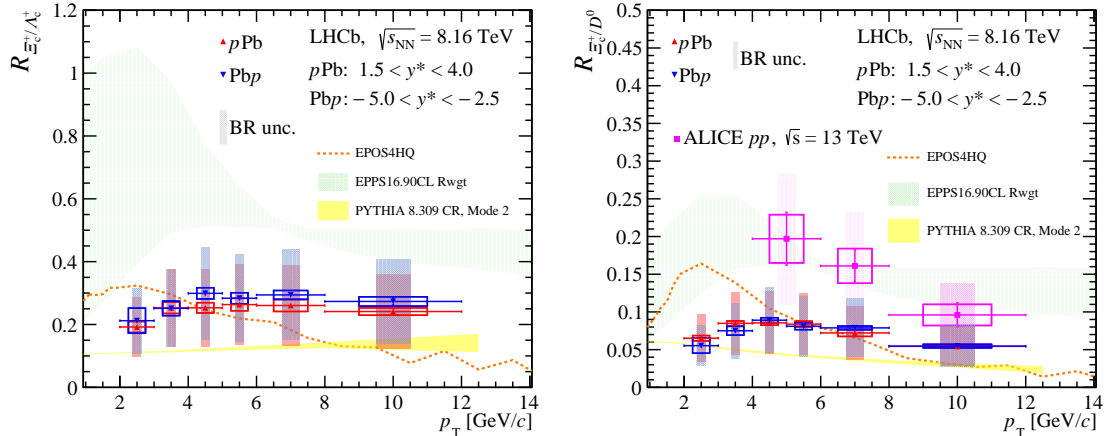


Figure 6: Ratio of (left) prompt Ξ_c^+ to Λ_c^+ production and (right) Ξ_c^+ to D^0 production in the p Pb (red triangles) and Pbp (blue triangles) data samples as a function of p_T . The error bars represent the statistical uncertainties, while the empty rectangles indicate the systematic uncertainty. Shaded rectangles denote the branching ratio uncertainty.

7 Summary

In summary, the prompt Ξ_c^+ production cross section in p Pb and Pbp collisions at a center-of-mass energy of $\sqrt{s_{NN}} = 8.16$ TeV at the LHCb experiment is measured differentially for the first time as a function of p_T and y^* . The cross section measurement provides new constraints for nPDF calculations, especially at low p_T , where the uncertainty on the factorisation scale is the largest. The forward-backward ratio R_{FB} is measured and found to be well described by nuclear shadowing calculations showing that there are no major final-state effects involved, in contrast to what has been observed in D^0 production studies in the same kinematic range at the same energy [56]. Prompt Ξ_c^+ production is compared to prompt Λ_c^+ production in the same kinematic region and their ratio is found to be constant within the uncertainties as a function of p_T and multiplicity, which is an indication that similar effects govern both Ξ_c^+ and Λ_c^+ production. The ratio of Ξ_c^+ to D^0 production is also measured as a function of p_T . Both ratios are found to be similar in p Pb and Pbp collisions but they show different trends compared to pp theory calculations. Therefore, our results show that hadronization in p Pb is not well understood and provides clear input for the hadronization studies in p Pb collisions.

Acknowledgements

We would like to thank to Hua-Sheng Shao, Jiaying Zhao and Joerg Aichelin for providing LHCb-specific theoretical predictions. We express our gratitude to our colleagues in the CERN accelerator departments for the excellent performance of the LHC. We thank the technical and administrative staff at the LHCb institutes. We acknowledge support from CERN and from the national agencies: CAPES, CNPq, FAPERJ and FINEP (Brazil); MOST and NSFC (China); CNRS/IN2P3 (France); BMBF, DFG and MPG (Germany); INFN (Italy); NWO (Netherlands); MNiSW and NCN (Poland); MCID/IFA (Romania); MICINN (Spain); SNSF and SER (Switzerland); NASU (Ukraine); STFC

(United Kingdom); DOE NP and NSF (USA). We acknowledge the computing resources that are provided by CERN, IN2P3 (France), KIT and DESY (Germany), INFN (Italy), SURF (Netherlands), PIC (Spain), GridPP (United Kingdom), CSCS (Switzerland), IFIN-HH (Romania), CBPF (Brazil), and Polish WLCG (Poland). We are indebted to the communities behind the multiple open-source software packages on which we depend. Individual groups or members have received support from ARC and ARDC (Australia); Key Research Program of Frontier Sciences of CAS, CAS PIFI, CAS CCEPP, Fundamental Research Funds for the Central Universities, and Sci. & Tech. Program of Guangzhou (China); Minciencias (Colombia); EPLANET, Marie Skłodowska-Curie Actions, ERC and NextGenerationEU (European Union); A*MIDEX, ANR, IPhU and Labex P2IO, and Région Auvergne-Rhône-Alpes (France); AvH Foundation (Germany); ICSC (Italy); GVA, XuntaGal, GENCAT, Inditex, InTalent and Prog. Atracción Talento, CM (Spain); SRC (Sweden); the Leverhulme Trust, the Royal Society and UKRI (United Kingdom).

A Additional plots

The differential ratios of Ξ_c^+ to Λ_c^+ and to D^0 production multiplied by $\mathcal{B}(\Xi_c^+ \rightarrow pK^-\pi^+)$ are shown in Figs. 7, 8, 9 and 10 as a function of p_T and y^* .

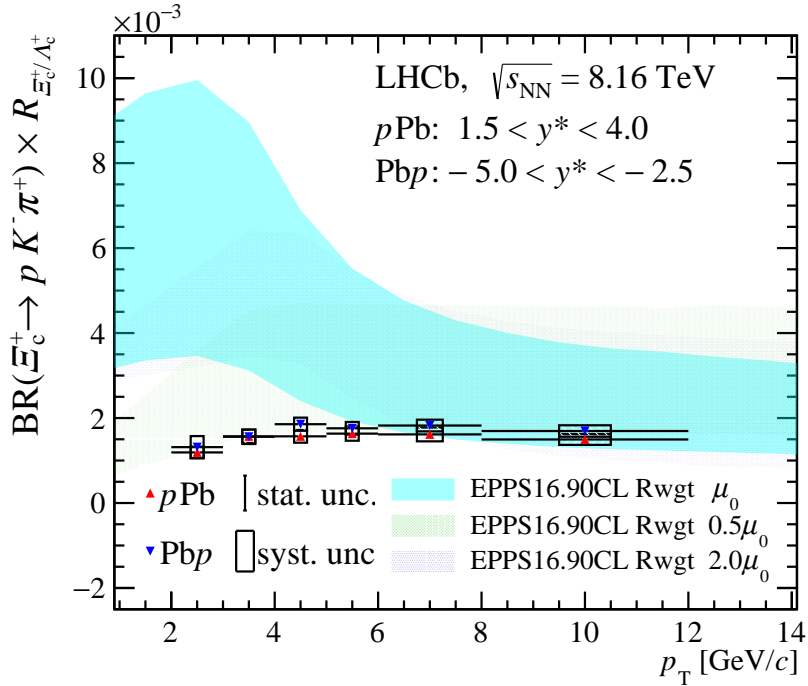


Figure 7: Production ratio of prompt Ξ_c^+ to Λ_c^+ baryons multiplied by $\mathcal{B}(\Xi_c^+ \rightarrow pK^-\pi^+)$ in $p\text{Pb}$ (red triangles) and $\text{Pb}p$ (blue triangles) data samples as a function of p_T . The error bars represent the statistical uncertainties while the squares indicate the systematic uncertainty.

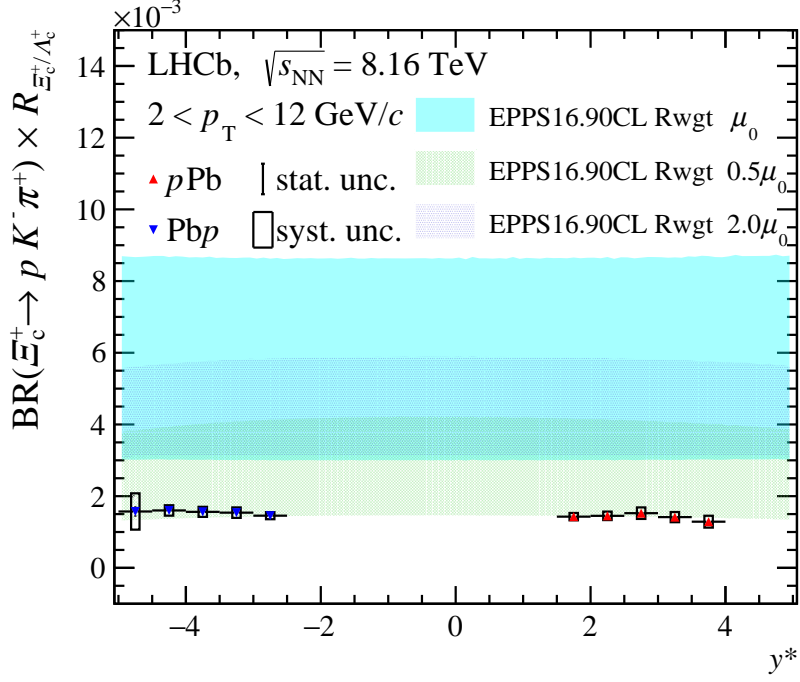


Figure 8: Production ratio of prompt Ξ_c^+ to Λ_c^+ baryons multiplied by $\mathcal{B}(\Xi_c^+ \rightarrow pK^-\pi^+)$ in $p\text{Pb}$ (red triangles) and $\text{Pb}p$ (blue triangles) data samples as a function of y^* . The error bars represent the statistical uncertainties while the squares indicate the systematic uncertainty.

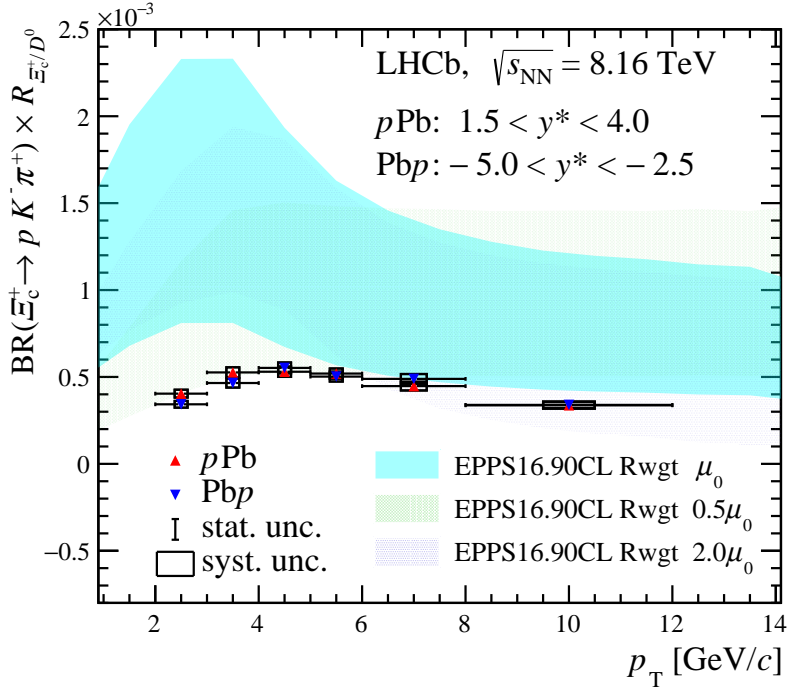


Figure 9: Production ratio of prompt Ξ_c^+ to D^0 baryons multiplied by $\mathcal{B}(\Xi_c^+ \rightarrow pK^-\pi^+)$ in $p\text{Pb}$ (red triangles) and $\text{Pb}p$ (blue triangles) data samples as a function of p_T . The error bars represent the statistical uncertainties while the squares indicate the systematic uncertainty.

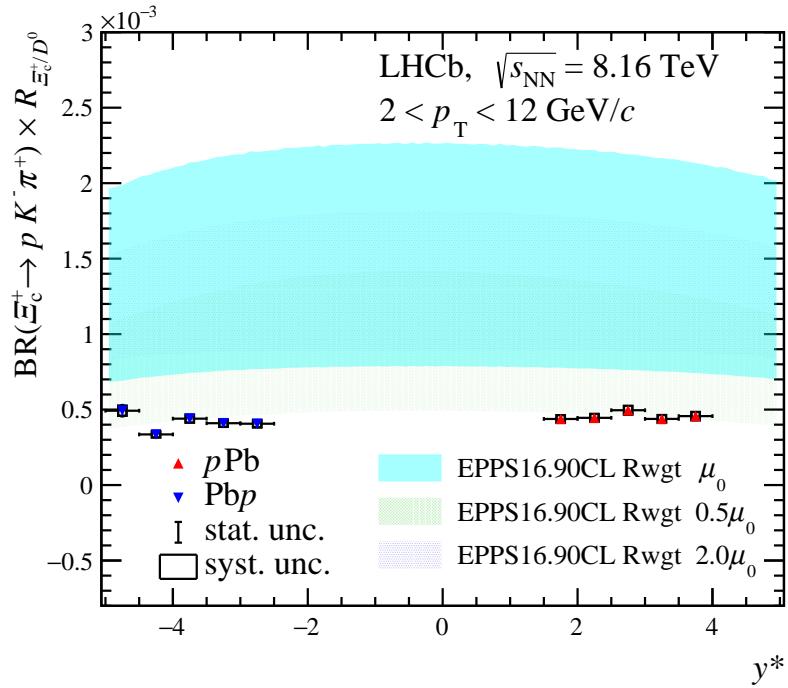


Figure 10: Production ratio of prompt Ξ_c^+ to D^0 baryons multiplied by $\mathcal{B}(\Xi_c^+ \rightarrow pK^-\pi^+)$ in $p\text{Pb}$ (red triangles) and Pbp (blue triangles) data samples as a function of y^* . The error bars represent the statistical uncertainties while the squares indicate the systematic uncertainty.

References

- [1] LHCb collaboration, R. Aaij *et al.*, *Measurements of prompt charm production cross-sections in pp collisions at $\sqrt{s} = 5$ TeV*, JHEP **06** (2017) 147, arXiv:1610.02230.
- [2] J. C. Collins, D. E. Soper, and G. F. Sterman, *Heavy particle production in high-energy hadron collisions*, Nucl. Phys. **B263** (1986) 37.
- [3] LHCb collaboration, R. Aaij *et al.*, *Measurement of b hadron production fractions in 7 TeV pp collisions*, Phys. Rev. **D85** (2012) 032008, arXiv:1111.2357.
- [4] K. Werner and B. Guiot, *Perturbative QCD concerning light and heavy flavor in the EPOS4 framework*, Phys. Rev. **C108** (2023) 034904, arXiv:2306.02396.
- [5] ALICE collaboration, S. Acharya *et al.*, *Λ_c^+ production in pp collisions at $\sqrt{s} = 7$ TeV and in p-Pb collisions at $\sqrt{s_{NN}} = 5.02$ TeV*, JHEP **04** (2018) 108, arXiv:1712.09581.
- [6] LHCb collaboration, R. Aaij *et al.*, *Prompt Λ_c^+ production in pPb collisions at $\sqrt{s_{NN}} = 5.02$ TeV*, JHEP **02** (2019) 102, arXiv:1809.01404.
- [7] ARGUS collaboration, H. Albrecht *et al.*, *Inclusive production of D^0 , D^+ and D^{*+} (2010) mesons in B decays and nonresonant e^+e^- annihilation at 10.6 GeV*, Z. Phys. **C52** (1991) 353.
- [8] CLEO collaboration, P. Avery *et al.*, *Inclusive production of the charmed baryon Λ_c^+ from e^+e^- annihilations at $\sqrt{s} = 10.55$ GeV*, Phys. Rev. **D43** (1991) 3599.
- [9] ZEUS collaboration, S. Chekanov *et al.*, *Measurement of charm fragmentation ratios and fractions in photoproduction at HERA*, Eur. Phys. J. **C44** (2005) 351, arXiv:hep-ex/0508019.
- [10] ZEUS collaboration, H. Abramowicz *et al.*, *Measurement of D^+ and Λ_c^+ production in deep inelastic scattering at HERA*, JHEP **11** (2010) 009, arXiv:1007.1945.
- [11] E. Braaten, K.-m. Cheung, S. Fleming, and T. C. Yuan, *Perturbative QCD fragmentation functions as a model for heavy quark fragmentation*, Phys. Rev. **D51** (1995) 4819, arXiv:hep-ph/9409316.
- [12] ALICE collaboration, S. Acharya *et al.*, *First measurement of Ξ_c^0 production in pp collisions at $\sqrt{s} = 7$ TeV*, Phys. Lett. **B781** (2018) 8, arXiv:1712.04242.
- [13] ALICE collaboration, S. Acharya *et al.*, *Measurement of the cross sections of Ξ_c^0 and Ξ_c^+ baryons and of the branching-fraction ratio $BR(\Xi_c^0 \rightarrow \Xi^- e^+ \nu_e)/BR(\Xi_c^0 \rightarrow \Xi^- \pi^+)$ in pp collisions at 13 TeV*, Phys. Rev. Lett. **127** (2021) 272001, arXiv:2105.05187.
- [14] J. R. Christiansen and P. Z. Skands, *String formation beyond leading colour*, JHEP **08** (2015) 003, arXiv:1505.01681.
- [15] V. Greco and C. M. Ko, *Hadronization via coalescence*, Acta Phys. Hung. **A24** (2005) 235, arXiv:nucl-th/0405040.
- [16] N. Armesto, *Nuclear shadowing*, J. Phys. **G32** (2006) R367, arXiv:hep-ph/0604108.













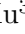

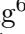






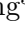
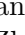
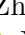
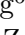
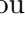
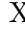



- [17] I. Vitev, *Non-Abelian energy loss in cold nuclear matter*, Phys. Rev. **C75** (2007) 064906, arXiv:hep-ph/0703002.
- [18] S. Gavin and J. Milana, *Energy loss at large x_f in nuclear collisions*, Phys. Rev. Lett. **68** (1992) 1834.
- [19] T. Dai, J.-F. Paquet, D. Teaney, and S. A. Bass, *Parton energy loss in a hard-soft factorized approach*, Phys. Rev. **C105** (2022) 034905, arXiv:2012.03441.
- [20] PHENIX collaboration, M. Wosocki, *Measurements of cold nuclear matter effects on J/ψ in the PHENIX experiment via deuteron-gold collisions*, J. Phys. **G35** (2008) 104069, arXiv:0804.4660.
- [21] R. Grajcarek, *Measurement of heavy-flavor production in Pb—Pb collisions at the LHC with ALICE*, Journal of Physics: Conference Series **420** (2013) 012032.
- [22] Y.-J. Lee, *Quark–gluon droplets engineered*, Nature Physics **15** (2019) 206.
- [23] J. Rafelski, *Strangeness production in the quark gluon plasma*, Nuclear Physics **A418** (1984) 215.
- [24] J. Rafelski, *Extreme states of nuclear matter.*, Nucl. Phys. **374** (1982) 489C.
- [25] P. Koch and J. Rafelski, *Time evolution of strange particle densities in hot hadronic matter*, Nucl. Phys. **A444** (1985) 678.
- [26] P. Koch, B. Muller, and J. Rafelski, *Strangeness in relativistic heavy ion collisions*, Phys. Rept. **142** (1986) 167.
- [27] J. Adam *et al.*, *Enhanced production of multi-strange hadrons in high-multiplicity proton–proton collisions*, Nature Physics **13** (2017) 535–539.
- [28] PHENIX collaboration, A. Adare *et al.*, *Spectra and ratios of identified particles in Au+Au and d+Au collisions at $\sqrt{s_{NN}} = 200$ GeV*, Phys. Rev. **C88** (2013) 024906, arXiv:1304.3410.
- [29] STAR collaboration, B. I. Abelev *et al.*, *Identified baryon and meson distributions at large transverse momenta from Au+Au collisions at $\sqrt{s_{NN}} = 200$ GeV*, Phys. Rev. Lett. **97** (2006) 152301, arXiv:nucl-ex/0606003.
- [30] LHCb collaboration, R. Aaij *et al.*, *Precision luminosity measurements at LHCb*, JINST **9** (2014) P12005, arXiv:1410.0149.
- [31] Particle Data Group, R. L. Workman *et al.*, *Review of particle physics*, Prog. Theor. Exp. Phys. **2022** (2022) 083C01.
- [32] LHCb collaboration, A. A. Alves Jr. *et al.*, *The LHCb detector at the LHC*, JINST **3** (2008) S08005.
- [33] LHCb collaboration, R. Aaij *et al.*, *LHCb detector performance*, Int. J. Mod. Phys. **A30** (2015) 1530022, arXiv:1412.6352.

- [34] R. Aaij *et al.*, *Performance of the LHCb Vertex Locator*, JINST **9** (2014) P09007, arXiv:1405.7808.
- [35] P. d'Argent *et al.*, *Improved performance of the LHCb Outer Tracker in LHC Run 2*, JINST **12** (2017) P11016, arXiv:1708.00819.
- [36] M. Adinolfi *et al.*, *Performance of the LHCb RICH detector at the LHC*, Eur. Phys. J. **C73** (2013) 2431, arXiv:1211.6759.
- [37] A. A. Alves Jr. *et al.*, *Performance of the LHCb muon system*, JINST **8** (2013) P02022, arXiv:1211.1346.
- [38] R. Aaij *et al.*, *The LHCb trigger and its performance in 2011*, JINST **8** (2013) P04022, arXiv:1211.3055.
- [39] T. Sjöstrand, S. Mrenna, and P. Skands, *A brief introduction to PYTHIA 8.1*, Comput. Phys. Commun. **178** (2008) 852, arXiv:0710.3820.
- [40] T. Pierog *et al.*, *EPOS LHC: Test of collective hadronization with data measured at the CERN Large Hadron Collider*, Phys. Rev. **C92** (2015) 034906, arXiv:1306.0121.
- [41] D. J. Lange, *The EvtGen particle decay simulation package*, Nucl. Instrum. Meth. **A462** (2001) 152.
- [42] Geant4 collaboration, S. Agostinelli *et al.*, *Geant4: A simulation toolkit*, Nucl. Instrum. Meth. **A506** (2003) 250.
- [43] Geant4 collaboration, J. Allison *et al.*, *Geant4 developments and applications*, IEEE Trans. Nucl. Sci. **53** (2006) 270.
- [44] G. Dujany and B. Storaci, *Real-time alignment and calibration of the LHCb Detector in Run II*, J. Phys. Conf. Ser. **664** (2015) 082010.
- [45] R. Aaij *et al.*, *Tesla: an application for real-time data analysis in High Energy Physics*, Comput. Phys. Commun. **208** (2016) 35, arXiv:1604.05596.
- [46] T. Skwarnicki, *A study of the radiative cascade transitions between the Upsilon-prime and Upsilon resonances*, PhD thesis, Institute of Nuclear Physics, Krakow, 1986, DESY-F31-86-02.
- [47] M. Pivk and F. R. Le Diberder, *sPlot: A statistical tool to unfold data distributions*, Nucl. Instrum. Meth. **A555** (2005) 356, arXiv:physics/0402083.
- [48] A. D. Bukin, *Fitting function for asymmetric peaks*, arXiv:0711.4449.
- [49] L. Anderlini *et al.*, *The PIDCalib package*, LHCb-PUB-2016-021, 2016.
- [50] J.-P. Lansberg and H.-S. Shao, *Towards an automated tool to evaluate the impact of the nuclear modification of the gluon density on quarkonium, D and B meson production in proton-nucleus collisions*, Eur. Phys. J. **C77** (2017) 1, arXiv:1610.05382.

- [51] A. Kusina, J.-P. Lansberg, I. Schienbein, and H.-S. Shao, *Gluon shadowing in heavy-flavor production at the LHC*, Phys. Rev. Lett. **121** (2018) 052004, [arXiv:1712.07024](#).
- [52] A. Kusina, J.-P. Lansberg, I. Schienbein, and H.-S. Shao, *Reweighted nuclear PDFs using heavy-flavor production data at the LHC*, Phys. Rev. **D104** (2021) 014010, [arXiv:2012.11462](#).
- [53] H.-S. Shao, *HELAC-Onia: An automatic matrix element generator for heavy quarkonium physics*, Comput. Phys. Commun. **184** (2013) 2562, [arXiv:1212.5293](#).
- [54] H.-S. Shao, *HELAC-Onia 2.0: An upgraded matrix-element and event generator for heavy quarkonium physics*, Comput. Phys. Commun. **198** (2016) 238, [arXiv:1507.03435](#).
- [55] K. J. Eskola, P. Paakkinen, H. Paukkunen, and C. A. Salgado, *EPPS16: Nuclear parton distributions with LHC data*, Eur. Phys. J. **C77** (2017) 163, [arXiv:1612.05741](#).
- [56] LHCb collaboration, R. Aaij *et al.*, *Measurement of the prompt D^0 nuclear modification factor in pPb collisions at $\sqrt{s_{NN}} = 8.16$ TeV*, Phys. Rev. Lett. **131** (2023) 102301, [arXiv:2205.03936](#).

LHCb collaboration

R. Aaij³² , A.S.W. Abdelmotteleb⁵⁰ , C. Abellan Beteta⁴⁴ , F. Abudinén⁵⁰ ,
 T. Ackernley⁵⁴ , B. Adeva⁴⁰ , M. Adinolfi⁴⁸ , P. Adlarson⁷⁷ , H. Afsharnia⁹ ,
 C. Agapopoulou¹³ , C.A. Aidala⁷⁸ , Z. Ajaltouni⁹ , S. Akar⁵⁹ , K. Akiba³² ,
 P. Albicocco²³ , J. Albrecht¹⁵ , F. Alessio⁴² , M. Alexander⁵³ , A. Alfonso Alberro³⁹ ,
 Z. Aliouche⁵⁶ , P. Alvarez Cartelle⁴⁹ , R. Amalric¹³ , S. Amato² , J.L. Amey⁴⁸ ,
 Y. Amhis^{11,42} , L. An⁴² , L. Anderlini²² , M. Andersson⁴⁴ , A. Andreianov³⁸ ,
 M. Andreotti²¹ , D. Andreou⁶² , D. Ao⁶ , F. Archilli^{31,t} , A. Artamonov³⁸ ,
 M. Artuso⁶² , E. Aslanides¹⁰ , M. Atzeni⁴⁴ , B. Audurier¹² , I.B. Bachiller Perea⁸ ,
 S. Bachmann¹⁷ , M. Bachmayer⁴³ , J.J. Back⁵⁰ , A. Bailly-reyre¹³ ,
 P. Baladron Rodriguez⁴⁰ , V. Balagura¹² , W. Baldini^{21,42} , J. Baptista de Souza Leite¹ ,
 M. Barbeti^{22,j} , R.J. Barlow⁵⁶ , S. Barsuk¹¹ , W. Barter⁵² , M. Bartolini⁴⁹ ,
 F. Baryshnikov³⁸ , J.M. Basels¹⁴ , G. Bassi^{29,q} , B. Batsukh⁴ , A. Battig¹⁵ ,
 A. Bay⁴³ , A. Beck⁵⁰ , M. Becker¹⁵ , F. Bedeschi²⁹ , I.B. Bediaga¹ , A. Beiter⁶² ,
 S. Belin⁴⁰ , V. Bellee⁴⁴ , K. Belous³⁸ , I. Belov³⁸ , I. Belyaev³⁸ , G. Benane¹⁰ ,
 G. Bencivenni²³ , E. Ben-Haim¹³ , A. Berezhnov³⁸ , R. Bernet⁴⁴ , S. Bernet Andres⁷⁶ ,
 D. Berninghoff¹⁷ , H.C. Bernstein⁶² , C. Bertella⁵⁶ , A. Bertolin²⁸ , C. Betancourt⁴⁴ ,
 F. Betti⁴² , Ia. Bezshyiko⁴⁴ , S. Bhasin⁴⁸ , J. Bhom³⁵ , L. Bian⁶⁸ , M.S. Bieker¹⁵ ,
 N.V. Biesuz²¹ , P. Billoir¹³ , A. Biolchini³² , M. Birch⁵⁵ , F.C.R. Bishop⁴⁹ ,
 A. Bitadze⁵⁶ , A. Bizzeti , M.P. Blago⁴⁹ , T. Blake⁵⁰ , F. Blanc⁴³ , J.E. Blank¹⁵ ,
 S. Blusk⁶² , D. Bobulska⁵³ , J.A. Boelhauve¹⁵ , O. Boente Garcia¹² , T. Boettcher⁵⁹ ,
 A. Boldyrev³⁸ , C.S. Bolognani⁷⁴ , R. Bolzonella^{21,i} , N. Bondar^{38,42} , F. Borgato²⁸ ,
 S. Borghi⁵⁶ , M. Borsato¹⁷ , J.T. Borsuk³⁵ , S.A. Bouchiba⁴³ , T.J.V. Bowcock⁵⁴ ,
 A. Boyer⁴² , C. Bozzi²¹ , M.J. Bradley⁵⁵ , S. Braun⁶⁰ , A. Brea Rodriguez⁴⁰ ,
 J. Brodzicka³⁵ , A. Brossa Gonzalo⁴⁰ , J. Brown⁵⁴ , D. Brundu²⁷ , A. Buonauro⁴⁴ ,
 L. Buonincontri²⁸ , A.T. Burke⁵⁶ , C. Burr⁴² , A. Bursche⁶⁶ , A. Butkevich³⁸ ,
 J.S. Butter³² , J. Buytaert⁴² , W. Byczynski⁴² , S. Cadeddu²⁷ , H. Cai⁶⁸ ,
 R. Calabrese^{21,i} , L. Calefice¹⁵ , S. Cali²³ , M. Calvi^{26,m} , M. Calvo Gomez⁷⁶ ,
 P. Campana²³ , D.H. Campora Perez⁷⁴ , A.F. Campoverde Quezada⁶ , S. Capelli^{26,m} ,
 L. Capriotti²⁰ , A. Carbone^{20,g} , R. Cardinale^{24,k} , A. Cardini²⁷ , P. Carniti^{26,m} ,
 L. Carus¹⁴ , A. Casais Vidal⁴⁰ , R. Caspary¹⁷ , G. Casse⁵⁴ , M. Cattaneo⁴² ,
 G. Cavallero^{55,42} , V. Cavallini^{21,i} , S. Celani⁴³ , J. Cerasoli¹⁰ , D. Cervenkov⁵⁷ ,
 A.J. Chadwick⁵⁴ , I.C. Chahrouh⁷⁸ , M.G. Chapman⁴⁸ , M. Charles¹³ , Ph. Charpentier⁴² ,
 C.A. Chavez Barajas⁵⁴ , M. Chefdeville⁸ , C. Chen¹⁰ , S. Chen⁴ , A. Chernov³⁵ ,
 S. Chernyshenko⁴⁶ , V. Chobanova⁴⁰ , S. Cholak⁴³ , M. Chrzaszcz³⁵ , A. Chubykin³⁸ ,
 V. Chulikov³⁸ , P. Ciambone²³ , M.F. Cicala⁵⁰ , X. Cid Vidal⁴⁰ , G. Ciezarek⁴² ,
 P. Cifra⁴² , G. Ciullo^{i,21} , P.E.L. Clarke⁵² , M. Clemencic⁴² , H.V. Cliff⁴⁹ ,
 J. Closier⁴² , J.L. Cobbledick⁵⁶ , V. Coco⁴² , J. Cogan¹⁰ , E. Cogneras⁹ ,
 L. Cojocariu³⁷ , P. Collins⁴² , T. Colombo⁴² , L. Congedo¹⁹ , A. Contu²⁷ ,
 N. Cooke⁴⁷ , I. Corredoira⁴⁰ , G. Corti⁴² , B. Couturier⁴² , D.C. Craik⁴⁴ ,
 M. Cruz Torres^{1,e} , R. Currie⁵² , C.L. Da Silva⁶¹ , S. Dadabaev³⁸ , L. Dai⁶⁵ ,
 X. Dai⁵ , E. Dall'Occo¹⁵ , J. Dalseno⁴⁰ , C. D'Ambrosio⁴² , J. Daniel⁹ ,
 A. Danilina³⁸ , P. d'Argent¹⁹ , J.E. Davies⁵⁶ , A. Davis⁵⁶ , O. De Aguiar Francisco⁵⁶ ,
 J. de Boer⁴² , K. De Bruyn⁷³ , S. De Capua⁵⁶ , M. De Cian⁴³ ,
 U. De Freitas Carneiro Da Graca¹ , E. De Lucia²³ , J.M. De Miranda¹ , L. De Paula² ,
 M. De Serio^{19,f} , D. De Simone⁴⁴ , P. De Simone²³ , F. De Vellis¹⁵ , J.A. de Vries⁷⁴ ,
 C.T. Dean⁶¹ , F. Debernardis^{19,f} , D. Decamp⁸ , V. Dedu¹⁰ , L. Del Buono¹³ ,
 B. Delaney⁵⁸ , H.-P. Dembinski¹⁵ , V. Denysenko⁴⁴ , O. Deschamps⁹ , F. Dettori^{27,h} ,
 B. Dey⁷¹ , P. Di Nezza²³ , I. Diachkov³⁸ , S. Didenko³⁸ , L. Dieste Maronas⁴⁰ ,

A.R. Wiederhold⁵⁰ , D. Wiedner¹⁵ , G. Wilkinson⁵⁷ , M.K. Wilkinson⁵⁹ , I. Williams⁴⁹,
M. Williams⁵⁸ , M.R.J. Williams⁵² , R. Williams⁴⁹ , F.F. Wilson⁵¹ , W. Wislicki³⁶ ,
M. Witek³⁵ , L. Witola¹⁷ , C.P. Wong⁶¹ , G. Wormser¹¹ , S.A. Wotton⁴⁹ , H. Wu⁶² ,
J. Wu⁷ , K. Wyllie⁴² , Z. Xiang⁶ , Y. Xie⁷ , A. Xu⁵ , J. Xu⁶ , L. Xu³ , L. Xu³ ,
M. Xu⁵⁰ , Q. Xu⁶, Z. Xu⁹ , Z. Xu⁶ , D. Yang³ , S. Yang⁶ , X. Yang⁵ , Y. Yang⁶ ,
Z. Yang⁵ , Z. Yang⁶⁰ , L.E. Yeomans⁵⁴ , V. Yeroshenko¹¹ , H. Yeung⁵⁶ , H. Yin⁷ ,
J. Yu⁶⁵ , X. Yuan⁶² , E. Zaffaroni⁴³ , M. Zavertyaev¹⁶ , M. Zdybal³⁵ , M. Zeng³ ,
C. Zhang⁵ , D. Zhang⁷ , L. Zhang³ , S. Zhang⁶⁵ , S. Zhang⁵ , Y. Zhang⁵ ,
Y. Zhang⁵⁷, Y. Zhao¹⁷ , A. Zharkova³⁸ , A. Zhelezov¹⁷ , Y. Zheng⁶ , T. Zhou⁵ ,
X. Zhou⁶ , Y. Zhou⁶ , V. Zhovkovska¹¹ , X. Zhu³ , X. Zhu⁷ , Z. Zhu⁶ ,
V. Zhukov^{14,38} , Q. Zou^{4,6} , S. Zucchelli^{20,9} , D. Zuliani²⁸ , G. Zunica⁵⁶ .

¹ *Centro Brasileiro de Pesquisas Físicas (CBPF), Rio de Janeiro, Brazil*

² *Universidade Federal do Rio de Janeiro (UFRJ), Rio de Janeiro, Brazil*

³ *Center for High Energy Physics, Tsinghua University, Beijing, China*

⁴ *Institute Of High Energy Physics (IHEP), Beijing, China*

⁵ *School of Physics State Key Laboratory of Nuclear Physics and Technology, Peking University, Beijing, China*

⁶ *University of Chinese Academy of Sciences, Beijing, China*

⁷ *Institute of Particle Physics, Central China Normal University, Wuhan, Hubei, China*

⁸ *Université Savoie Mont Blanc, CNRS, IN2P3-LAPP, Annecy, France*

⁹ *Université Clermont Auvergne, CNRS/IN2P3, LPC, Clermont-Ferrand, France*

¹⁰ *Aix Marseille Univ, CNRS/IN2P3, CPPM, Marseille, France*

¹¹ *Université Paris-Saclay, CNRS/IN2P3, IJCLab, Orsay, France*

¹² *Laboratoire Leprince-Ringuet, CNRS/IN2P3, Ecole Polytechnique, Institut Polytechnique de Paris, Palaiseau, France*

¹³ *LPNHE, Sorbonne Université, Paris Diderot Sorbonne Paris Cité, CNRS/IN2P3, Paris, France*

¹⁴ *I. Physikalisches Institut, RWTH Aachen University, Aachen, Germany*

¹⁵ *Fakultät Physik, Technische Universität Dortmund, Dortmund, Germany*

¹⁶ *Max-Planck-Institut für Kernphysik (MPIK), Heidelberg, Germany*

¹⁷ *Physikalisches Institut, Ruprecht-Karls-Universität Heidelberg, Heidelberg, Germany*

¹⁸ *School of Physics, University College Dublin, Dublin, Ireland*

¹⁹ *INFN Sezione di Bari, Bari, Italy*

²⁰ *INFN Sezione di Bologna, Bologna, Italy*

²¹ *INFN Sezione di Ferrara, Ferrara, Italy*

²² *INFN Sezione di Firenze, Firenze, Italy*

²³ *INFN Laboratori Nazionali di Frascati, Frascati, Italy*

²⁴ *INFN Sezione di Genova, Genova, Italy*

²⁵ *INFN Sezione di Milano, Milano, Italy*

²⁶ *INFN Sezione di Milano-Bicocca, Milano, Italy*

²⁷ *INFN Sezione di Cagliari, Monserrato, Italy*

²⁸ *Università degli Studi di Padova, Università e INFN, Padova, Padova, Italy*

²⁹ *INFN Sezione di Pisa, Pisa, Italy*

³⁰ *INFN Sezione di Roma La Sapienza, Roma, Italy*

³¹ *INFN Sezione di Roma Tor Vergata, Roma, Italy*

³² *Nikhef National Institute for Subatomic Physics, Amsterdam, Netherlands*

³³ *Nikhef National Institute for Subatomic Physics and VU University Amsterdam, Amsterdam, Netherlands*

³⁴ *AGH - University of Science and Technology, Faculty of Physics and Applied Computer Science, Kraków, Poland*

³⁵ *Henryk Niewodniczanski Institute of Nuclear Physics Polish Academy of Sciences, Kraków, Poland*

³⁶ *National Center for Nuclear Research (NCBJ), Warsaw, Poland*

³⁷ *Horia Hulubei National Institute of Physics and Nuclear Engineering, Bucharest-Magurele, Romania*

³⁸ *Affiliated with an institute covered by a cooperation agreement with CERN*

³⁹ *ICCUB, Universitat de Barcelona, Barcelona, Spain*

- ⁴⁰ *Instituto Galego de Física de Altas Enerxías (IGFAE), Universidade de Santiago de Compostela, Santiago de Compostela, Spain*
- ⁴¹ *Instituto de Física Corpuscular, Centro Mixto Universidad de Valencia - CSIC, Valencia, Spain*
- ⁴² *European Organization for Nuclear Research (CERN), Geneva, Switzerland*
- ⁴³ *Institute of Physics, Ecole Polytechnique Fédérale de Lausanne (EPFL), Lausanne, Switzerland*
- ⁴⁴ *Physik-Institut, Universität Zürich, Zürich, Switzerland*
- ⁴⁵ *NSC Kharkiv Institute of Physics and Technology (NSC KIPT), Kharkiv, Ukraine*
- ⁴⁶ *Institute for Nuclear Research of the National Academy of Sciences (KINR), Kyiv, Ukraine*
- ⁴⁷ *University of Birmingham, Birmingham, United Kingdom*
- ⁴⁸ *H.H. Wills Physics Laboratory, University of Bristol, Bristol, United Kingdom*
- ⁴⁹ *Cavendish Laboratory, University of Cambridge, Cambridge, United Kingdom*
- ⁵⁰ *Department of Physics, University of Warwick, Coventry, United Kingdom*
- ⁵¹ *STFC Rutherford Appleton Laboratory, Didcot, United Kingdom*
- ⁵² *School of Physics and Astronomy, University of Edinburgh, Edinburgh, United Kingdom*
- ⁵³ *School of Physics and Astronomy, University of Glasgow, Glasgow, United Kingdom*
- ⁵⁴ *Oliver Lodge Laboratory, University of Liverpool, Liverpool, United Kingdom*
- ⁵⁵ *Imperial College London, London, United Kingdom*
- ⁵⁶ *Department of Physics and Astronomy, University of Manchester, Manchester, United Kingdom*
- ⁵⁷ *Department of Physics, University of Oxford, Oxford, United Kingdom*
- ⁵⁸ *Massachusetts Institute of Technology, Cambridge, MA, United States*
- ⁵⁹ *University of Cincinnati, Cincinnati, OH, United States*
- ⁶⁰ *University of Maryland, College Park, MD, United States*
- ⁶¹ *Los Alamos National Laboratory (LANL), Los Alamos, NM, United States*
- ⁶² *Syracuse University, Syracuse, NY, United States*
- ⁶³ *School of Physics and Astronomy, Monash University, Melbourne, Australia, associated to ⁵⁰*
- ⁶⁴ *Pontifícia Universidade Católica do Rio de Janeiro (PUC-Rio), Rio de Janeiro, Brazil, associated to ²*
- ⁶⁵ *Physics and Micro Electronic College, Hunan University, Changsha City, China, associated to ⁷*
- ⁶⁶ *Guangdong Provincial Key Laboratory of Nuclear Science, Guangdong-Hong Kong Joint Laboratory of Quantum Matter, Institute of Quantum Matter, South China Normal University, Guangzhou, China, associated to ³*
- ⁶⁷ *Lanzhou University, Lanzhou, China, associated to ⁴*
- ⁶⁸ *School of Physics and Technology, Wuhan University, Wuhan, China, associated to ³*
- ⁶⁹ *Departamento de Física, Universidad Nacional de Colombia, Bogotá, Colombia, associated to ¹³*
- ⁷⁰ *Universität Bonn - Helmholtz-Institut für Strahlen und Kernphysik, Bonn, Germany, associated to ¹⁷*
- ⁷¹ *Eotvos Lorand University, Budapest, Hungary, associated to ⁴²*
- ⁷² *INFN Sezione di Perugia, Perugia, Italy, associated to ²¹*
- ⁷³ *Van Swinderen Institute, University of Groningen, Groningen, Netherlands, associated to ³²*
- ⁷⁴ *Universiteit Maastricht, Maastricht, Netherlands, associated to ³²*
- ⁷⁵ *Faculty of Material Engineering and Physics, Cracow, Poland, associated to ³⁵*
- ⁷⁶ *DS4DS, La Salle, Universitat Ramon Llull, Barcelona, Spain, associated to ³⁹*
- ⁷⁷ *Department of Physics and Astronomy, Uppsala University, Uppsala, Sweden, associated to ⁵³*
- ⁷⁸ *University of Michigan, Ann Arbor, MI, United States, associated to ⁶²*

^a *Universidade de Brasília, Brasília, Brazil*

^b *Central South U., Changsha, China*

^c *Hangzhou Institute for Advanced Study, UCAS, Hangzhou, China*

^d *Excellence Cluster ORIGINS, Munich, Germany*

^e *Universidad Nacional Autónoma de Honduras, Tegucigalpa, Honduras*

^f *Università di Bari, Bari, Italy*

^g *Università di Bologna, Bologna, Italy*

^h *Università di Cagliari, Cagliari, Italy*

ⁱ *Università di Ferrara, Ferrara, Italy*

^j *Università di Firenze, Firenze, Italy*

^k *Università di Genova, Genova, Italy*

^l *Università degli Studi di Milano, Milano, Italy*

^m *Università di Milano Bicocca, Milano, Italy*

ⁿ *Università di Modena e Reggio Emilia, Modena, Italy*

- ^o *Università di Padova, Padova, Italy*
^p *Università di Perugia, Perugia, Italy*
^q *Scuola Normale Superiore, Pisa, Italy*
^r *Università di Pisa, Pisa, Italy*
^s *Università della Basilicata, Potenza, Italy*
^t *Università di Roma Tor Vergata, Roma, Italy*
^u *Università di Urbino, Urbino, Italy*
^v *Universidad de Alcalá, Alcalá de Henares , Spain*
[†] *Deceased*